

# Journal of Geophysical Research: Oceans

## RESEARCH ARTICLE

10.1002/2017JC013324

**Key Points:**

- Interannual trends of chlorophyll-*a* were similar nearshore and offshore in the Southern California Bight
- Chlorophyll increased and shoaled before 2006–2010 and decreased and deepened after
- Observed trends are linked to low-frequency climatic cycles

**Supporting Information:**

- Supporting Information S1

**Correspondence to:**

N. P. Nezlin,  
nezlin@scwrp.org

**Citation:**

Nezlin, N. P., McLaughlin, K., Booth, J. A. T., Cash, C. L., Diehl, D. W., Davis, K. A., ... Weisberg, S. B. (2018). Spatial and temporal patterns of chlorophyll concentration in the Southern California Bight. *Journal of Geophysical Research: Oceans*, 123. <https://doi.org/10.1002/2017JC013324>

Received 9 AUG 2017

Accepted 15 DEC 2017

Accepted article online 27 DEC 2017

## Spatial and Temporal Patterns of Chlorophyll Concentration in the Southern California Bight

Nikolay P. Nezlin<sup>1</sup> , Karen McLaughlin<sup>1</sup> , J. Ashley T. Booth<sup>2</sup>, Curtis L. Cash<sup>2</sup>, Dario W. Diehl<sup>1</sup> , Kristen A. Davis<sup>3</sup>, Adriano Feit<sup>4</sup>, Ralf Goericke<sup>5</sup>, Joseph R. Gully<sup>6</sup>, Meredith D. A. Howard<sup>1</sup>, Scott Johnson<sup>7</sup>, Ami Latker<sup>4</sup>, Michael J. Mengel<sup>8</sup>, George L. Robertson<sup>8</sup>, Alex Steele<sup>6</sup>, Laura Terriquez<sup>8</sup>, Libe Washburn<sup>9</sup> , and Stephen B. Weisberg<sup>1</sup> 

<sup>1</sup>Southern California Coastal Water Research Project Authority, Costa Mesa, CA, USA, <sup>2</sup>City of Los Angeles, Bureau of Sanitation, Playa del Rey, CA, USA, <sup>3</sup>Henry Samueli School of Engineering, University of California, Irvine, Irvine, CA, USA,

<sup>4</sup>Public Utilities Department, City of San Diego, San Diego, CA, USA, <sup>5</sup>Scripps Institution of Oceanography, La Jolla, CA, USA,

<sup>6</sup>Sanitation Districts of Los Angeles County (LACSD), Whittier, CA, USA, <sup>7</sup>Aquatic Bioassay Consulting Laboratories, Ventura, CA, USA, <sup>8</sup>Orange County Sanitation District (OCSD), Fountain Valley, CA, USA, <sup>9</sup>Marine Science Institute, University of California, Santa Barbara, Santa Barbara, CA, USA

**Abstract** Distinguishing between local, anthropogenic nutrient inputs and large-scale climatic forcing as drivers of coastal phytoplankton biomass is critical to developing effective nutrient management strategies. Here we assess the relative importance of these two drivers by comparing trends in chlorophyll-*a* between shallow coastal (0.1–16.5 km) and deep offshore (17–700 km) areas, hypothesizing that coastal regions influenced by anthropogenic nutrient inputs may have different spatial and temporal patterns in chlorophyll-*a* concentration from offshore regions where coastal inputs are less influential. Quarterly conductivity-temperature-depth (CTD) fluorescence measurements collected from three southern California continental shelf regions since 1998 were compared to chlorophyll-*a* data from the more offshore California Cooperative Fisheries Investigations (CalCOFI) program. The trends in the coastal zone were similar to those offshore, with a gradual increase of chlorophyll-*a* biomass and shallowing of its maximum layer since the beginning of observations, followed by chlorophyll-*a* declining and deepening from 2010 to present. An exception was the northern coastal part of SCB, where chlorophyll-*a* continued increasing after 2010. The long-term increase in chlorophyll-*a* prior to 2010 was correlated with increased nitrate concentrations in deep waters, while the recent decline was associated with deepening of the upper mixed layer, both linked to the low-frequency climatic cycles of the Pacific Decadal Oscillation and North Pacific Gyre Oscillation. These large-scale factors affecting the physical structure of the water column may also influence the delivery of nutrients from deep ocean outfalls to the euphotic zone, making it difficult to distinguish the effects of anthropogenic inputs on chlorophyll along the coast.

### 1. Introduction

Remotely sensed ocean color data suggest that phytoplankton biomass has been increasing along the southern California coast over the last two decades (Kahru et al., 2012; Nezlin et al., 2012). Such increases may result from local nutrient inputs (Howard et al., 2014), but can also result from large-scale climate forcing (Cloern, 2001). For instance, natural processes like strengthening of wind-generated coastal upwelling (Bakun, 1990; Bakun et al., 2010; Di Lorenzo, 2015) and increased nutrient concentrations in deep source waters (Bograd et al., 2015; Rykaczewski & Dunne, 2010) can affect frequency and magnitude of algal blooms nearshore. Large-scale climatic drivers affecting phytoplankton biomass in the northeastern Pacific include warming-enhanced stratification and decreased productivity (Behrenfeld et al., 2006; Polovina et al., 2008). Other climatic drivers include low-frequency events such as the El-Niño Southern Oscillation (ENSO) (Philander, 1990; Trenberth, 1997) and regime shifts thereof (Hayward et al., 1999; Kim & Miller, 2007; Miller & Schneider, 2000; Peterson & Schwing, 2003), and climatic cycles like the Pacific Decadal Oscillation (PDO) (Mantua et al., 1997; Newman et al., 2016) and the North Pacific Gyre Oscillation (NPGO) (Di Lorenzo et al., 2008).

The ocean's physical environment has a strong control over phytoplankton biomass response. Phytoplankton growth is regulated by the availability of light and nutrients, with most nutrient supply to well-illuminated

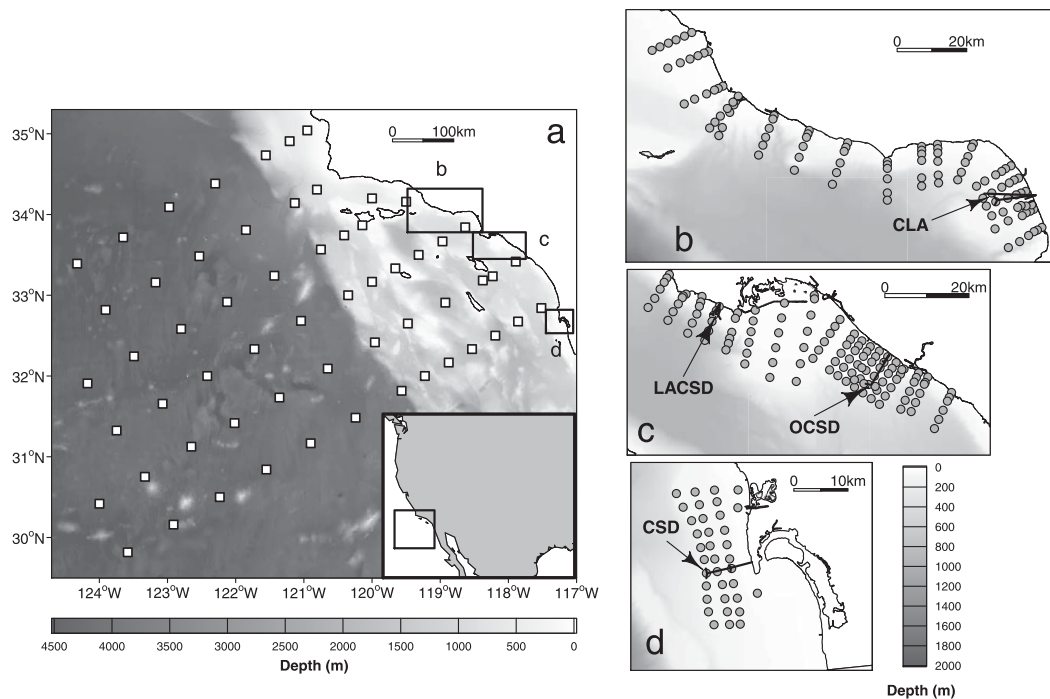


**Figure 1.** (a) CalCOFI stations and the (b) northern; (c) central; (d) southern coastal SCB regions where CTD profiles were collected during POTW WQ monitoring. Arrows point at the four major wastewater outfalls in SCB: City of Los Angeles (CLA), Sanitation Districts of Los Angeles County (LACSD), Orange County Sanitation District (OCSD), and City of San Diego (CSD).

surface ocean coming from the mixing and upwelling of cold, nutrient-rich water from below (Dugdale, 1967; Riley, 1946). Enhanced stratification can suppress nutrient exchange through vertical mixing, while surface cooling favors elevated vertical exchange which may result in greater primary productivity (Behrenfeld et al., 2006; Longhurst, 1995).

Differentiating between the effects of local eutrophication associated with coastal anthropogenic nutrient inputs and climate forcing is important for successful coastal resource management. Here, we assess the relative importance of these two drivers by comparing chlorophyll-*a* trends in three coastal regions of the Southern California Bight (SCB) subject to anthropogenic nutrient inputs, with trends farther offshore, where shore-based nutrients additions are unlikely to play a significant role. Specifically, we examine interannual trends in chlorophyll vertical structure and physical environment in the nearshore zone (0.1–16.5 km offshore) with the offshore region (17–700 km) utilizing decades-long records of in situ observations of chlorophyll to better understand the relative role of large-scale remote versus local controls on the long-term trends in phytoplankton biomass in the SCB.

## 2. Material and Methods

### 2.1. Study Area

The SCB is the bend in the coastline between Point Conception (~34° 34'N) and the Mexico international border (~32° 32'N) (Figure 1). The physical circulation in the SCB is dominated by the equatorward California Current (CC), a typical eastern boundary current, transporting cold Subarctic water from north to south (Hickey, 1979; Lynn & Simpson, 1987). To the south of Point Conception, the coastline turns eastward forming the northern part of the SCB, which is sheltered from the direct effect of upwelling-generating winds by a coastal mountain range (Dorman, 1982). The poleward current along the coast, the Southern California Countercurrent (Sverdrup & Fleming, 1941), transports warm southern water as far north as the Santa Monica Basin and the Santa Barbara Channel. The SCB is bordered by a narrow shelf, typically 3–6 km wide, but as far as 12 km in some areas. The bottom topography of SCB consists of ranges of submarine mountains and valleys resulting in unsteady, complex circulation patterns (Hickey, 1992, 1993; Lynn & Simpson, 1987).

Southern California is a highly populated, semiarid region with low surface runoff that is confined mostly to the winter rainy season. Wastewater discharge is the dominant source of terrestrially derived nutrients to the SCB, with four large municipal wastewater treatment facilities (Publicly Owned Treatment Works, POTWs) discharging a large amount of nitrogen ( $6.5 \cdot 10^3$ – $16 \cdot 10^3$  metric tons per year each) (Lyon et al., 2006), significantly exceeding other terrestrial sources (Howard et al., 2014; Lyon & Stein, 2008). Billions of dollars have been invested over the past three decades in reducing pollutant emissions in that area, resulting in substantial improvement in aquatic communities (Stein & Cadien, 2009). At the same time, the area has shown a decline in oxygen content (Booth et al., 2014) and an increase in acidification (Leinweber & Gruber, 2013). It is unclear to what degree these changes are driven by basin-scale forcing and/or local anthropogenic nutrient inputs.

## 2.2. Data Collection

Nearshore SCB chlorophyll fluorescence profiles were measured quarterly at 258 stations along 49 cross-shelf transects from summer 1998 to fall 2015 in the northern and central SCB and from fall 2003 to fall 2015 in the southern SCB (Figure 1). CTDs were deployed to 100 m depth, or to 2 m above the bottom at stations with less than 100 m depth, measuring a suite of ocean properties including pressure, temperature, salinity, colored dissolved organic matter, dissolved oxygen, and chlorophyll fluorescence. The resulting profiles were averaged to 1 m bins. Sampling was conducted by five Publicly Owned Treatment Works (POTW) agencies during their regulatory monitoring, each using their own instruments and vessels: Aquatic Bioassay and Consulting Laboratories, Inc., representing the City of Oxnard (Oxnard), City of Los Angeles (CLA), Los Angeles County Sanitation Districts (LACSD), Orange County Sanitation District (OCSD), and City of San Diego (CSD). For analysis, we grouped data regionally, Oxnard and CLA as the northern region, LACSD and OCSD as the central region, and CSD as the southern coastal region (Figure 1).

Chlorophyll fluorescence measurements were made with WET Labs WETStar (WS3S) fluorometers, which were calibrated annually by the manufacturer. Conversion of chlorophyll fluorescence to chlorophyll-*a* concentration (CHL) was based on 357 discrete CHL samples collected from the surface and the maximum CHL fluorescence layer in parallel to CTD profiles in winter 2009 (70 samples), winter 2010 (24 samples), spring 2010 (211 samples), and spring 2013 (52 samples). Calibration samples were collected in the morning to minimize the effect of diurnal variations of CHL fluorescence yield. CHL was extracted in 90% acetone and measured with a Turner 10-AU fluorometer using the acidification method (Parsons et al., 1984). CHL bottle samples were compared to CTD CHL measurements averaged within 5 m layers. A power-law relationship between discrete CHL concentration ( $\text{mg m}^{-3}$ ) and fluorescence (volts) was developed from these data:

$$[\text{CHL} = 5.8423 \cdot V^{1.0649}], \quad (1)$$

and applied to all data since 2009. A power-law relationship was preferred over linear because statistical distribution of CHL in the ocean is typically close to lognormal (Banse & English, 1994; Campbell, 1995). The relationship demonstrated high correlation ( $R^2 = 0.677$ ) and was equally applicable to all southern California regions and observation periods (no significant differences were detected by ANOVA).

Prior to 2009, historical CTD data sets did not include voltage for CHL fluorescence and consequently the above relationship could not be applied. For these data CHL concentrations ( $\text{mg m}^{-3}$ ) were calculated from fluorescence using standard linear coefficients provided by the manufacturer. Factory calibration ensures the scaling factor correctly responds to internal standards and reference lab culture of *Thalassiosira weissflogii* phytoplankton used by the manufacturer, in addition to setting the clean water offset. However, comparison of the CHL concentration reported using the manufacturer calibration and discrete bottle samples collected as calibration for this study showed that the manufacturer calibration significantly overestimated chlorophyll concentrations in the SCB. Consequently, a correction factor of 0.4 was calculated and applied to the historical data collected by all five agencies. This factor was estimated as the averaged difference between all CHL bottle samples and collected at the same stations as the factory-calibrated CTD CHL measurements. This difference in methodology converting fluorescence to chlorophyll concentration may have influenced the results. However, for the northern and central regions, the pre-2009 and post-2009 appear to be reasonably well aligned, while the data for the southern region had an abrupt change, which may be due to this change in methodology rather than chlorophyll biomass. Therefore, we interpreted pre-2009 data with caution.

Oceanographic observations offshore of southern California have been carried out for almost 70 years by the CalCOFI program ([www.calcofi.org](http://www.calcofi.org)). Since 1984, concentrations of inorganic nutrients and CHL, as well as basic hydrographic variables, have been measured on a quarterly basis at 66 stations off Southern California. To avoid overlap of the regions, we used in this study 59 stations in the area 17–700 km offshore (referred below as the CalCOFI region) (Figure 1a). Data at each station included in situ water samples collected by 10 L plastic Niskin bottles. Bottle samples were typically taken at 20 depths, generally chosen to provide a high resolution (~10 m) around steep gradient features such as the subsurface CHL maximum. Temperature, salinity, and inorganic nutrients (including nitrate) were measured for all depths sampled. CHL samples were taken within the upper 200 m and CHL was determined from the fluorescence of acetone extracts (Parsons et al., 1984). Further details of the sampling and analytical procedures can be found at [www.calcofi.org](http://www.calcofi.org).

### 2.3. Analytical Metrics

Two metrics were used to assess spatial and temporal trends in magnitude and vertical structure of phytoplankton biomass at each station. To ascertain changes in the magnitude of biomass, we calculated vertically integrated CHL concentration of the water column (0–200 m for CalCOFI and 0–100 m for POTW data)  $\text{CHL}_{\text{tot}}$  (mg CHL m<sup>-2</sup>)

$$\text{CHL}_{\text{tot}} = \int \text{CHL}(z) \cdot dz \quad (2)$$

using the trapezoidal rule with basepoints  $\text{CHL}(z)$ , which is CHL concentration (mg CHL m<sup>-3</sup>) at depth Z.

To evaluate changes in vertical structure, we calculated the depth of the CHL profiles' center of mass,  $D_{\text{chl}}$  (m):

$$D_{\text{chl}} (\text{m}) = \frac{1}{\text{CHL}_{\text{tot}}} \cdot \int z \cdot \text{CHL}(z) \cdot dz \quad (3)$$

Center of mass was preferred over the more traditional chlorophyll maximum depth (cf. Cullen, 2015) because many nearshore profiles had two (or more) subsurface peaks in chlorophyll fluorescence or broad maximum peaks, making classification of a single "maximum" depth layer difficult.

We investigated three metrics to characterize the relationship between the ocean physical environment and  $\text{CHL}_{\text{tot}}$  and  $D_{\text{chl}}$  in the SCB: (1) water column stratification regulating nutrient flux into the euphotic zone, (2) nutrient concentration in deeper waters, (3) horizontal advection of waters with different nutrient content associated with large-scale ocean circulation patterns ("nutrient-rich" waters transported from the north versus "nutrient-poor" waters from the south). To assess the covariance of deep-water nutrients with CHL, the nitracline depth ( $D_{\text{nc}}$ ) was calculated as the depth where nitrate concentrations started increasing with depth from near-zero (<0.1  $\mu\text{M L}^{-1}$ ) values (calculated for CalCOFI data only). The depth of the potential density anomaly ( $\sigma_0$ ) 25.0 kg m<sup>-3</sup> isopycnal ( $D_{\sigma 25}$ ) was used as a proxy for water column stratification. Isopycnal surface 25.0 kg m<sup>-3</sup> was selected because this density was measured in most profiles of both CalCOFI and POTW data sets, and could thus be used as a characteristic of water column density profiles.  $D_{\sigma 25}$  was preferred to other measures of water column stratification (buoyancy frequency and the pycnocline depth calculated using different methods [Freeland et al., 1997; Papadakis, 1981; Thomson & Fine, 2003]), which demonstrated poor relationship with  $\text{CHL}_{\text{tot}}$  and  $D_{\text{chl}}$ . Spiciness  $\pi$  (a state variable orthogonal to density (Flament, 2002), is often used as a tracer of basin-scale water mass movements. We analyzed spiciness ( $\pi_{\sigma 25}$ ) and nitrate concentrations ( $\text{NO}_3_{\sigma 25}$ ) at the  $D_{\sigma 25}$  depth. All oceanographic parameters were calculated using the R package "oce" (Kelley & Richards, 2017). The spatial distributions and temporal variations of the basic metrics averaged over the four studied regions are given in supporting information Figures S1–S11.

### 2.4. Statistical Analysis

Temporal trends, and regions where these trends occurred, were assessed using Empirical Orthogonal Functions (EOFs) (Emery & Thomson, 2014; Preisendorfer, 1988). EOFs decompose time series of spatial maps (here time series of  $\text{CHL}_{\text{tot}}$ ,  $D_{\text{chl}}$ , etc. over the sampling patterns from the three POTW regions and one CalCOFI region) into a set of orthogonal functions, or modes. These modes consist of two parts: (1) maps of spatial distributions of a variable for each mode; and (2) a time series that quantifies how each map changes in time. In the procedure, each parameter  $\psi_m(t)$  (e.g.,  $\text{CHL}_{\text{tot}}$ ) at each station (m) and time (t) was normalized as

$$\psi'_m(t) = [\psi_m(t) - \bar{\psi}_m]/\sigma_m \quad (4)$$

where  $\bar{\psi}_m$  and  $\sigma_m$  are the mean and standard deviation over all observations at station  $m$ . Variations of each parameter were separated into modes as,

$$\psi'_m(t) = \sum_i^M a'_i(t) \cdot \varphi_{im} \quad (5)$$

where  $a'_i(t)$  is the amplitude function of mode  $i$  for observation  $t$ ;  $\varphi_{im}$  is spatial mode  $i$  at station  $m$ ; summation is over all  $M$  modes. Spatial modes  $\varphi_{ij}$  are orthogonal and amplitude functions  $a'_i(t)$  are uncorrelated. The modes are ranked according to the fraction of variance accounted for each mode in the original data. Often a few modes explain much of the variance for a given parameter. Missing data were reconstructed using the Data Interpolating Empirical Orthogonal Functions (DINEOF) approach (Beckers & Rixen, 2003) implemented in the R package "spacetime" (Pebesma, 2012). Normalized amplitude functions  $a'_i(t)$  obtained using equation (5) were transformed to dimensional amplitude functions  $a_i(t)$  by regressing them against the original data set.

EOF analysis was applied independently to the three coastal SCB regions and the offshore CalCOFI region. For all parameters, only the first EOF mode ( $m = 1$ ) was analyzed because it captured the fundamental variability of the system (27–94% of the variance depending on the parameter). Other EOF modes were not analyzed because they explained less variance and did not exhibit clear spatial patterns through time.

Maps of the each variable's first EOF mode were generated using Barnes algorithm (Koch et al., 1983) implemented in the R package "oce" (Kelley & Richards, 2017). To keep the interpolated variables realistic outside the contour of the sampled region, a number of "artificial stations" were placed at the distance 100 km (CalCOFI) or 10 km (POTW) from the "boundary" of the sampled region, with the values at these locations made close to the values at the nearby stations in the region contour. The latter was achieved by using the "Inverse Distance Weighted" method with a power parameter 4.0 ("idw" function from the R package "gstat" (Pebesma, 2004).

The periods when trends were statistically significant were detected using Generalized Additive Models (GAM), a method based on optimal smoothing of the time series. GAM is a nonparametric generalization of the linear regression model (Hastie & Tibshirani, 1986), where the usual linear function of a covariate is replaced with a sum of unspecified smooth functions determined by the data through iterative smoothing operations. After the GAM model was fitted for each seasonally adjusted time series using R package "mgcv" (Wood, 2016), the derivatives (slopes) and their standard errors (confidence intervals) were computed for each predicted point using the method of finite differences using an unofficial R package "tsgam" (available from <https://github.com/gavinsimpson/tsgam>) (Simpson, 2017). The periods when these derivatives were significantly different from zero at the selected confidence level were defined as statistically significant trends (Simpson, 2014). The points between the increasing and decreasing periods were detected as the points where the slope is zero. A salient feature of most observed parameters was the change of the trend direction observed between 2006 and 2010. Significance of the trends before and after this change was estimated by detecting the time when the change occurred preceding the most recent period of significant change and estimating the significance of the linear trends before and after this time.

## 2.5. Influence of Large-Scale Climatic Forcing on Local CHL Expression

The effect of climate fluctuations on the CHL biomass and vertical structure was analyzed using the PDO (Mantua et al., 1997; Newman et al., 2016) and NPGO (Di Lorenzo et al., 2008) indices obtained from the websites <http://research.jisao.washington.edu/pdo/PDO.latest> and <http://www.ices.us/npgc/npgc.php>.

## 3. Results

### 3.1. CHL Biomass and Vertical Structure Nearshore and Offshore

Interannual variations of  $CHL_{tot}$  and  $D_{chl}$  nearshore and offshore generally demonstrated similar, but inverse, features. Offshore, in the CalCOFI region,  $CHL_{tot}$  increased and  $D_{chl}$  shoaled from the beginning of regular observations in 1984 to ~2006, followed by a decrease of  $CHL_{tot}$  starting in 2006 and a deepening of the  $D_{chl}$  starting in 2010 (Figure 2). On average,  $CHL_{tot}$  in the CalCOFI region increased from  $34 \text{ mg m}^{-2}$  in 1984 to  $55 \text{ mg m}^{-2}$  in 2006 and then decreased to  $43 \text{ mg m}^{-2}$  in 2015. The decrease since 2010 of  $CHL_{tot}$

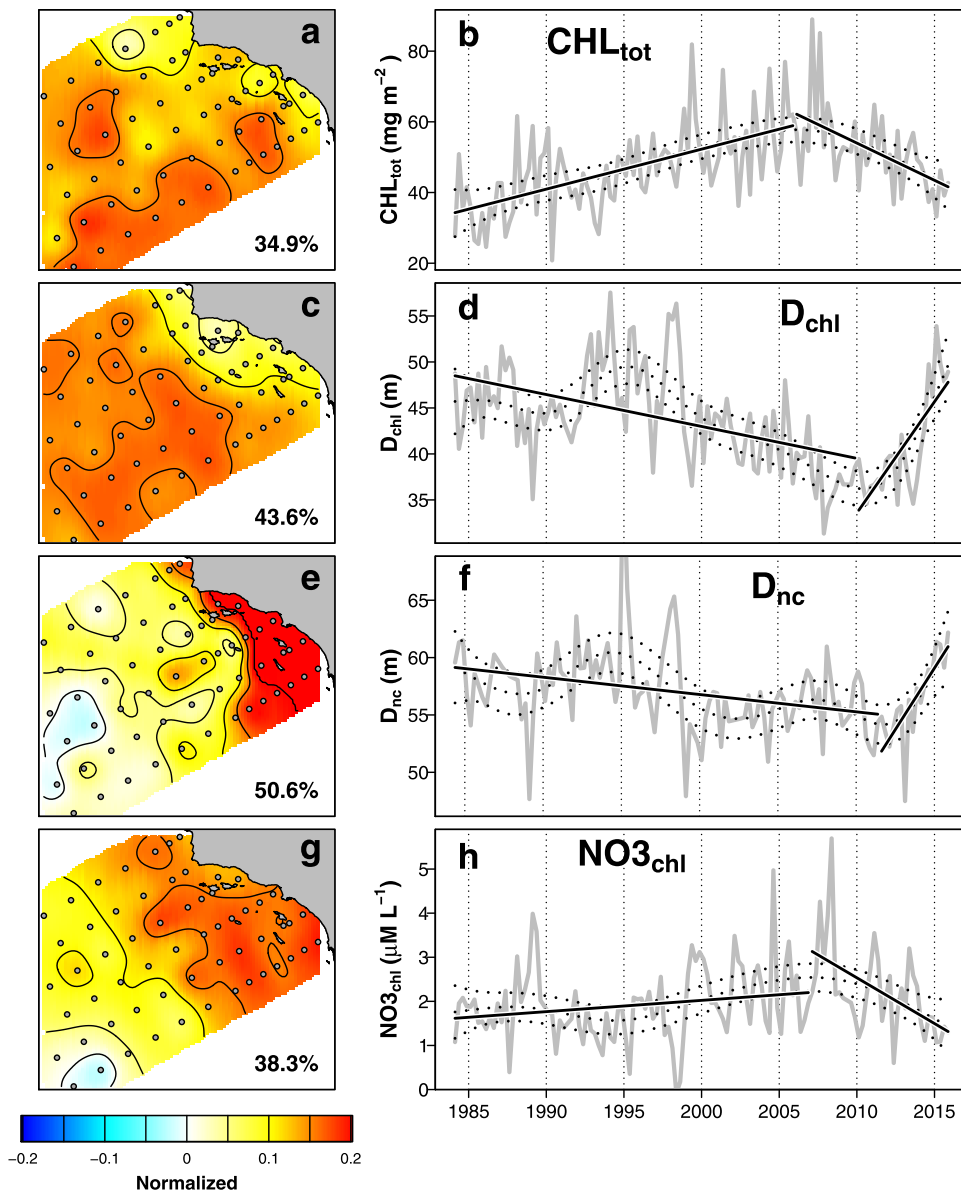


**Figure 2.** (a, c, e, g) Spatial distributions and (b, d, f, h) temporal variations of first EOF modes of integrated CHL ( $\text{CHL}_{\text{tot}}$ ), CHL center of mass depth ( $D_{\text{chl}}$ ), the depth of nitracline  $D_{\text{nc}}$  and nitrate concentration ( $\text{NO}_3_{\text{chl}}$ ) at the  $D_{\text{chl}}$  depth in CalCOFI region. The percent of variance explained by each mode is given at corner of the map. All time series are smoothed using GAM method (dashed lines show the mean and the 0.95 confidence interval). Black lines indicate the periods of significant ( $p < 0.05$ ) linear trends.

was also observed in the central and southern coastal SCB (Figures 3c–3f), where  $\text{CHL}_{\text{tot}}$  decreased from 75–170 mg m<sup>-2</sup> in 2010 to 45–59 mg m<sup>-2</sup> in 2015, but not in the northern SCB where values continued to increase from 32 mg m<sup>-2</sup> in 1998 to 110 mg m<sup>-2</sup> in 2015 (Figure 3b). No significant increase of  $\text{CHL}_{\text{tot}}$  before 2010 was observed in the central and southern regions (Figures 3c–3f). Analyzing  $\text{CHL}_{\text{tot}}$  trends nearshore, we must consider the difference between the methods of CHL biomass assessment before and after 2009. The continuity in the time series of  $\text{CHL}_{\text{tot}}$  in the northern and central SCB suggests there may not be a bias from the methodological differences (Figures 3b and 3d). However, in the southern region, the lack of continuity between data sets suggests it could be the reason for the abrupt  $\text{CHL}_{\text{tot}}$  increase between 2008 and 2010 (Figure 3f).

The deepening of  $D_{\text{chl}}$  after 2006–2010 observed offshore (Figure 2d) was also observed in all three coastal regions (Figure 4). In the northern and central coastal regions,  $D_{\text{chl}}$  was 18–21 m in 2006–2011 and

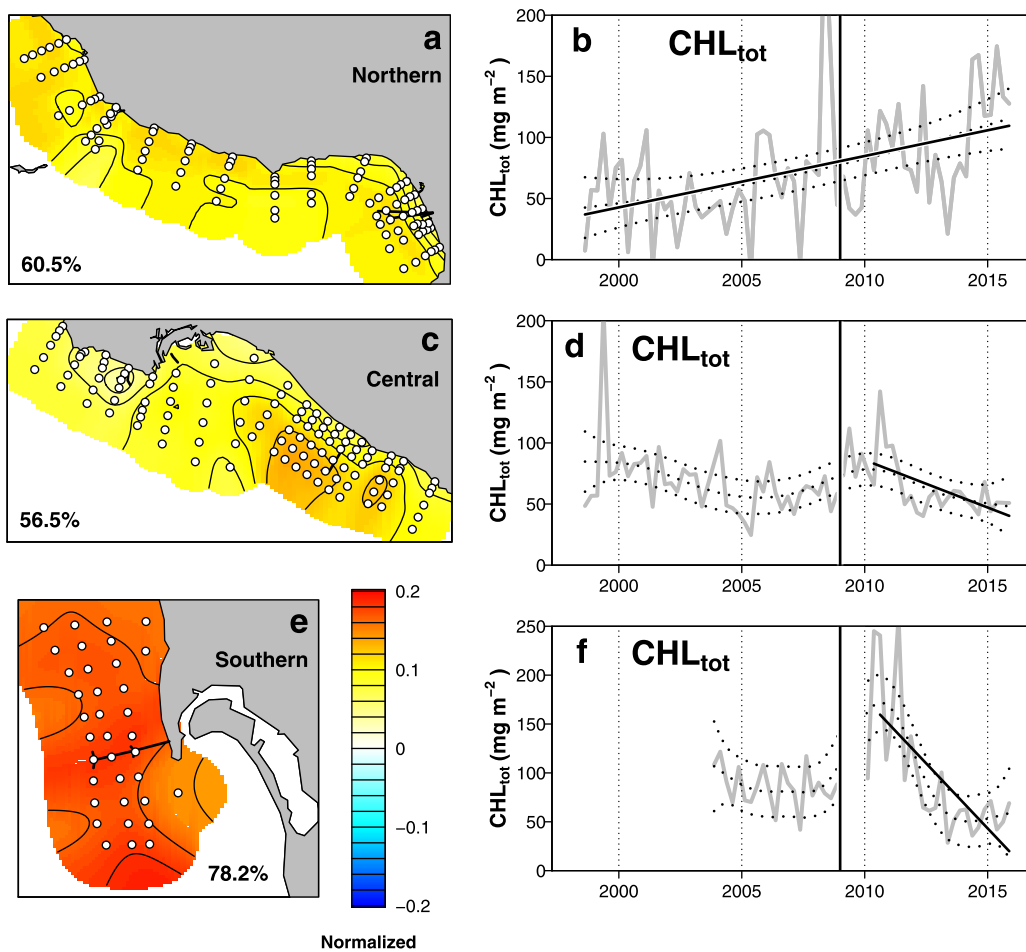


**Figure 3.** (a, c, e) Spatial distributions and (b, d, f) temporal variations of first EOF modes of the integrated CHL ( $\text{CHL}_{\text{tot}}$ ) in (a, b) northern, (c, d) central and (e, f) southern coastal regions (POTW data set). The percent of variance explained by each mode is given at corner of the map. All time series are smoothed using GAM method (dashed lines show the mean and the 0.95 confidence interval). Black lines indicate the periods of significant ( $p < 0.05$ ) linear trend. Vertical lines indicate the time (2009) when the method of CHL calculation was changed.

deepened to 22–25 m in 2015 (Figures 4b and 4d), whereas in the southern region  $D_{\text{chl}}$  deepened from 25 m in 2008–2011 to 36 m in 2015 (Figure 4f). In the CalCOFI region,  $D_{\text{chl}}$  deepened from 36 m in 2010 to 48–50 m in 2015 (Figure 2d). Before 2010, significant shallowing of the  $D_{\text{chl}}$  was observed offshore and in the central coastal SCB (Figures 2d and 4d). In the northern and southern SCB this trend was insignificant (Figures 4a, 4b, 4e, and 4f), possibly due to the short period of observations. Spatial distribution of the first EOF mode of  $D_{\text{chl}}$  in the CalCOFI region demonstrated higher variability offshore than nearshore (Figure 2c).

### 3.2. Relationship With Nutrients

Patterns in subsurface chlorophyll were highly correlated with nutrient availability in the offshore region (this could not be assessed from the nearshore POTW data set because nitrate data were not collected). Changes in  $\text{CHL}_{\text{tot}}$  and  $D_{\text{chl}}$  during 1984–2010 covaried with the nitrate concentrations at the  $D_{\text{chl}}$  depth and the depth of the nitracline (Figure 2). In the CalCOFI area, the depths of  $D_{\text{chl}}$  and  $D_{\text{nc}}$  were significantly positively correlated ( $R^2 = 0.70$ ;  $d.f. = 5,500$ ; correlation based on all profiles where  $D_{\text{chl}}$  and  $D_{\text{nc}}$  were detected), both demonstrating shallowing during 1984–2010 and deepening around 1995 and after 2010. Furthermore, a gradual increase in nitrate concentration at the  $D_{\text{chl}}$  during 1984–2008 (Figure 2h) also coincided with increasing  $\text{CHL}_{\text{tot}}$ .

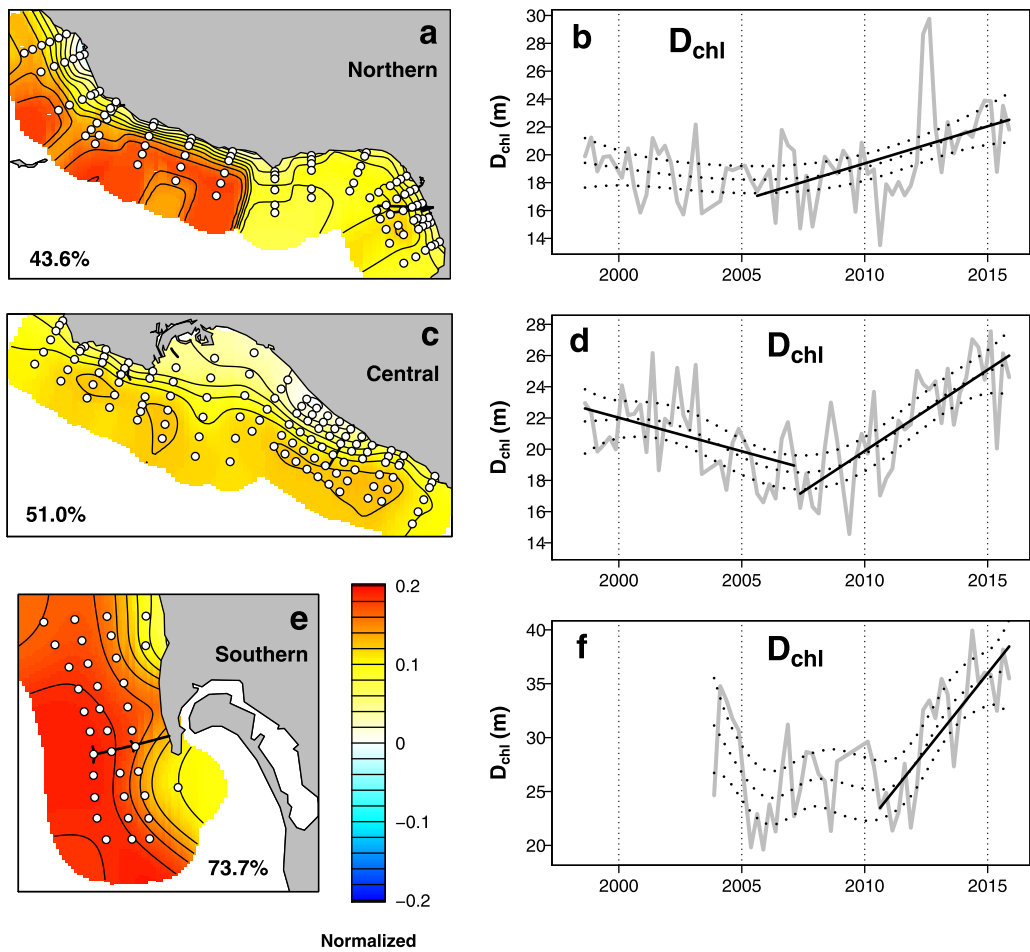


**Figure 4.** (a, c, e) Spatial distributions and (b, d, f) temporal variations of first EOF modes of the CHL center of mass depth ( $D_{chl}$ ) in (a, b) northern, (c, d) central, and (e, f) southern coastal regions (POTW data set). The percent of variance explained by each mode is given at corner of the map. All time series are smoothed using GAM method (dashed lines show the mean and the 0.95 confidence interval). Black lines indicate the periods of significant ( $p < 0.05$ ) linear trend.

### 3.3. Relationship With the Ocean Physical Environment

We investigated three metrics to characterize the relationship between the ocean physical environment and spatial and temporal patterns in CHL<sub>tot</sub> and D<sub>chl</sub> in the SCB: (1) water column stratification regulating nutrient flux into the euphotic zone, represented by the depth of the  $\sigma_{25}$  isopycnal, D <sub>$\sigma_{25}$</sub> , (2) horizontal advection of waters with different spiciness and nutrient content associated with large-scale ocean circulation patterns (cold/fresh/"nutrient-rich" waters transported from the north versus warm/salty/"nutrient-poor" waters from the south), as reflected by spiciness on the  $\sigma_{25}$  isopycnal,  $\pi_{\sigma_{25}}$ , and (3) nutrient concentration in deeper waters, represented by the metric NO3 <sub>$\sigma_{25}$</sub> .

Water column stratification, as interpreted through the isopycnal surface 25.0 kg m<sup>-3</sup>, D <sub>$\sigma_{25}$</sub>  (Figures 5e, 5f and 6), covaried with observed patterns in CHL<sub>tot</sub> and D<sub>chl</sub> (Figures 2b and 2d) after 2010 but not before. D <sub>$\sigma_{25}$</sub>  was comparatively stable with two periods of deepening: about 1995–2000 (offshore) and 2010–2015 (all four data sets); D <sub>$\sigma_{25}$</sub>  variations in the CalCOFI region were more pronounced nearshore than offshore (Figure 5e). Both periods of deepening of the D <sub>$\sigma_{25}$</sub>  coincided with deepening of the D<sub>chl</sub> (Figures 2b and 4) and the nitracline D<sub>nc</sub> (Figure 2f), although only the recent (2010–2015) deepening resulted in a decrease of CHL<sub>tot</sub> (Figures 2b, 3d, and 3f).

Advection of waters of different origin, as interpreted through the metric spiciness,  $\pi_{\sigma_{25}}$ , did not seem to be associated with patterns in CHL<sub>tot</sub> and D<sub>chl</sub>. Temporal variations of  $\pi_{\sigma_{25}}$  offshore and nearshore were similar (Figures 5a, 5b, and 7), but there was no clear relationship between spiciness and CHL<sub>tot</sub> and D<sub>chl</sub> (cf. Figures

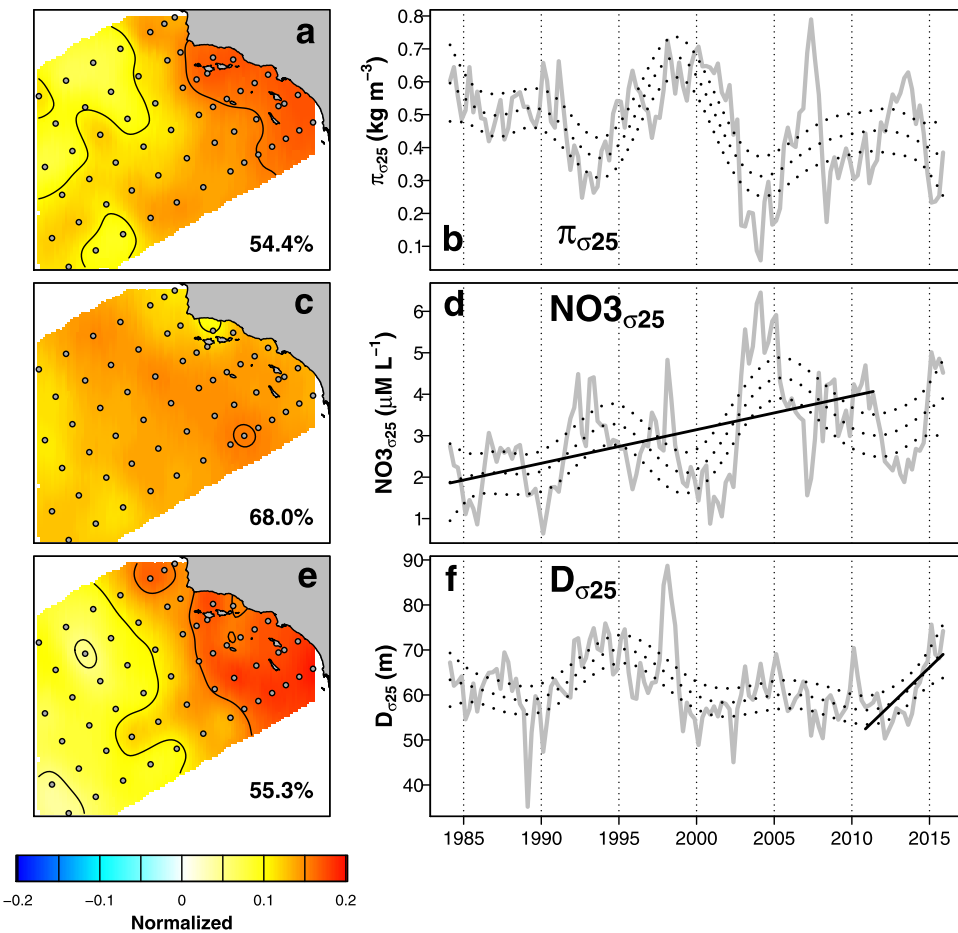


**Figure 5.** (a, c, e, g) Spatial distributions and (b, d, f, h) temporal variations of first EOF modes of (a, b) spiciness  $\pi_{\sigma 25}$  and (c, d) nitrate concentration  $\text{NO}_3_{\sigma 25}$  at the depth of the  $25.0 \text{ kg m}^{-3}$  isopycnal and (e, f) the depth  $D_{\sigma 25}$  of this isopycnal (CalCOFI data set). The percent of variance explained by each mode is given at corner of the map. All time series are smoothed using GAM method (dashed lines show the mean and the 0.95 confidence interval). Black lines indicate the periods of significant ( $p < 0.05$ ) linear trend.

2b, 2d, 3, and 4). In contrast to  $\text{CHL}_{\text{tot}}$  and  $D_{\text{chl}}$ ,  $\pi_{\sigma 25}$  demonstrated no significant linear trends during the observed period. Neither the spiciness maximum that occurred in 1997–1998 (associated with the strongest El Niño in the 20th century) nor the two spiciness minima in 1993 and 2004 were associated with maxima in either  $\text{CHL}_{\text{tot}}$  and  $D_{\text{chl}}$ .

Nitrate concentrations measured at the isopycnal surface  $25.0 \text{ kg m}^{-3}$ ,  $\text{NO}_3_{\sigma 25}$ , demonstrated two independent temporal patterns (Figure 5d). First, it was inversely correlated with spiciness, confirming the idea that cold/fresh waters advected from the north are rich in nutrients in contrast to warm/salty waters advected from the south. Corresponding temporal variations, however, are not seen in the  $\text{CHL}_{\text{tot}}$  and  $D_{\text{chl}}$ . Second, the nitrate concentrations at this depth (which was 10–30 m nearshore and 50–70 m offshore) significantly increased from 1984 to 2005 (Figure 5d), also observed as an increase in nitrate concentration at the depth of  $D_{\text{chl}}$  (Figure 2h).

#### 4. Discussion

The SCB, as a part of an eastern boundary current system, is strongly affected by seasonal coastal upwelling and the California Current transporting productive waters from the Subarctic Pacific (Hickey, 1979; Lynn & Simpson, 1987). Others have noted that phytoplankton productivity in eastern boundary systems results from a combined effect of large-scale circulation and local factors (Carr & Kearns, 2003), and that multiple factors such as nutrient concentration, light availability, and water mass mixing can affect phytoplankton

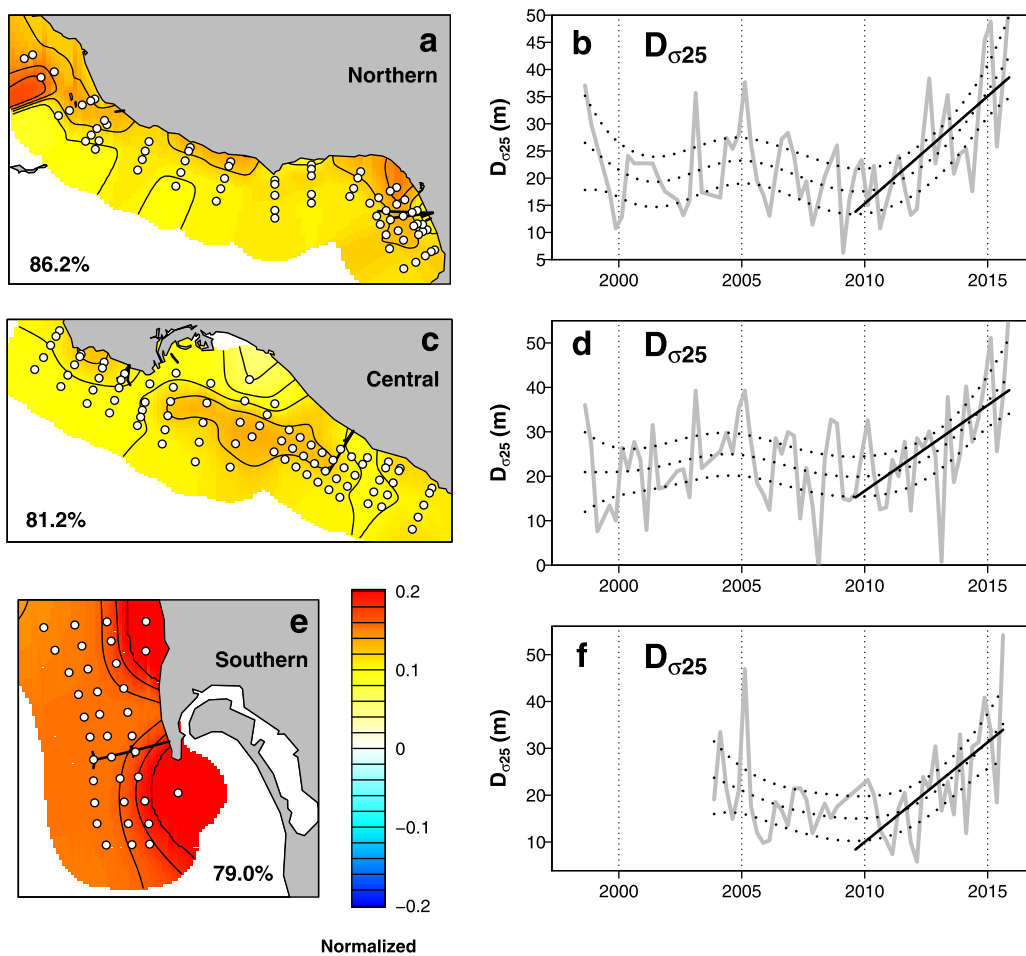


**Figure 6.** (a, c, e) Spatial distributions and (b, d, f) temporal variations of first EOF modes of the depth of the  $25.0 \text{ kg m}^{-3}$  isopycnal ( $D_{\sigma 25}$ ) in the (a, b) northern, (c, d) central, and (e, f) southern coastal regions (POTW data set). The percent of variance explained by each mode is given at corner of the map. All time series are smoothed using GAM method (dashed lines show the mean and the 0.95 confidence interval). Black lines indicate the periods of significant ( $p < 0.05$ ) linear trend.

distribution (Messie & Chavez, 2015; Patti et al., 2008). The concurrence of nearshore and offshore trends in CHL biomass ( $\text{CHL}_{\text{tot}}$ ) and vertical structure ( $D_{\text{chl}}$ ) and their association with water column stratification ( $D_{\sigma 25}$ ) and deep-water nitrate concentrations suggest that nearshore subsurface CHL patterns are driven largely by Pacific Basin-scale climate events.

Increasing CHL concentrations and shallowing of  $D_{\text{chl}}$  in the SCB during most of the observed period (1984–2010) appear to be linked to a shallowing of the nitractine (Aksnes & Ohman, 2009; Bjorkstedt et al., 2011; McClatchie et al., 2016) and higher nitrate concentrations of deep waters that source upwelling (Bjorkstedt et al., 2012; Bograd et al., 2015). Deep ocean nutrients are becoming enriched as a result of global changes related to ocean warming, including decreased ventilation of the North Pacific, more intensive remineralization at depth, and longer time for the water masses to accrue nitrate below the euphotic zone during their transits from the subarctic to the subtropics (Rykaczewski & Dunne, 2010). In the SCB, the effect of warming is different from the trends observed further offshore, where an increase in surface temperatures and stratification suppress nutrient supply to the euphotic zone making them less productive (Behrenfeld et al., 2006; Polovina et al., 2011; Roemmich & McGowan, 1995; Sarmiento et al., 2004; Steinacher et al., 2010).

The patterns in  $\text{CHL}_{\text{tot}}$  and  $D_{\text{chl}}$  and the associated physical factors appear to be linked to PDO and NPGO climatic cycles, which are forced responses of the ocean to atmospheric variability generated by the El Niño Southern Oscillation (ENSO) fluctuations in the Equatorial Pacific (Di Lorenzo et al., 2013). PDO and NPGO

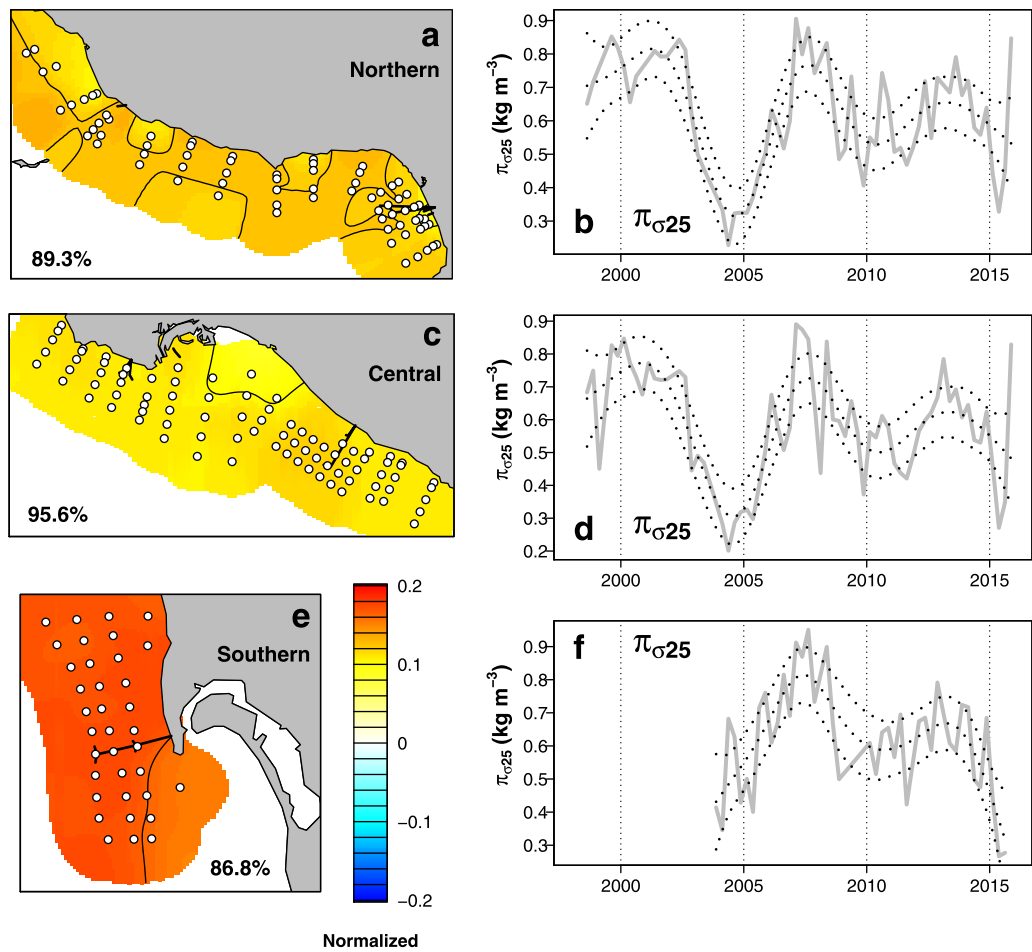


**Figure 7.** (a, c, e) Spatial distributions and (b, d, f) temporal variations of first EOF modes of spiciness at the depth of the  $25.0 \text{ kg m}^{-3}$  ( $\pi_{025}$ ) in the (a, b) northern, (c, d) central, and (e, f) southern coastal regions (POTW data set). The percent of variance explained by each mode is given at corner of the map. All time series are smoothed using GAM method (dashed lines show the mean and the 0.95 confidence interval). Black lines indicate the periods of significant ( $p < 0.05$ ) linear trend.

both drive upwelling, water transport, mixing, mesoscale structure, and ecosystem dynamics in the northeastern Pacific (Di Lorenzo et al., 2009, 2013; Kilduff et al., 2015; Mantua et al., 1997). The NPGO (defined as the second mode of sea surface height anomalies) is associated with the strength of the central and eastern parts of the North Pacific gyre circulations, including the California Current (Di Lorenzo et al., 2008), transporting productive ocean waters from the north. Previous studies demonstrated significant correlation between the NPGO index and surface chlorophyll- $\alpha$  (Di Lorenzo et al., 2008) and nitrate concentration in the upper mixed layer (Di Lorenzo et al., 2009) averaged over the CalCOFI domain. The PDO (the leading mode of sea surface temperature variability in the North Pacific) covaries with different aspects of ocean ecosystems from Alaska to California, including salmon production regimes, continental surface air temperatures, major costal river flow, etc. (Mantua et al., 1997). In the northeastern Pacific Ocean, the periods of positive ("warm") PDO phases are associated with an El Niño-like increase of sea surface temperature, deepening of the pycnocline, and a decrease of primary production; while negative ("cold") PDO has an opposite effect (Chao et al., 2000; Wang et al., 2014; Zhang et al., 1997). The most pronounced effects on the ocean ecosystem (often called "physical-biological regime shifts") have occurred when the PDO and NPGO show strong, simultaneous, and opposite sign reversals (Di Lorenzo et al., 2008).

During 1984–2010, both climatic indices (seasonally adjusted and smoothed by the GAM method) demonstrated small but significant trends (decreasing PDO and increasing NPGO) overlaid by quasiperiodic decadal oscillations (Figure 8). In the SCB, both these trends are associated with increased primary

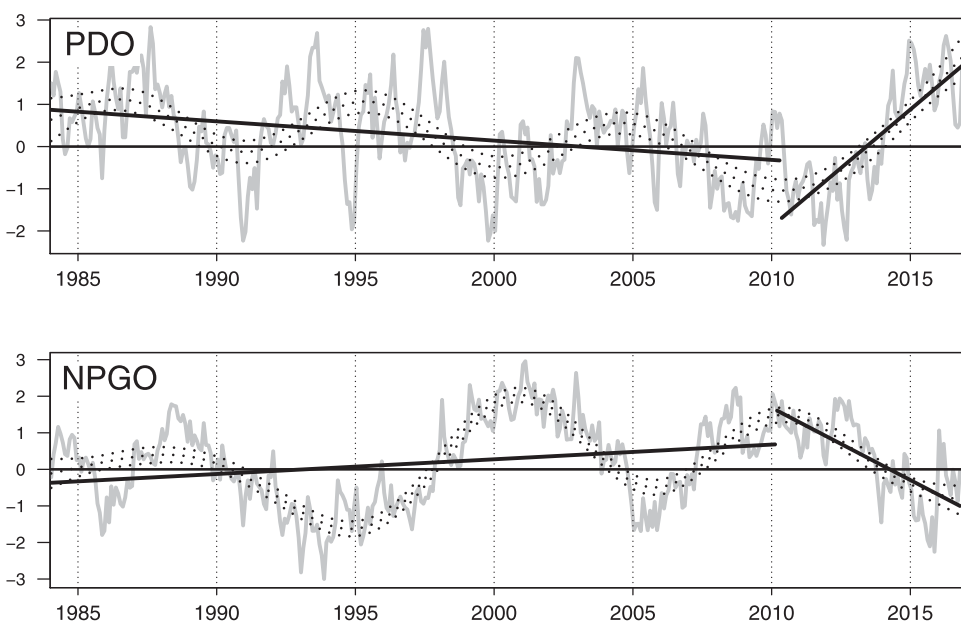


**Figure 8.** Pacific Decadal Oscillation (PDO) and North Pacific Gyre Oscillation (NPGO) smoothed by GAM method (dashed lines show mean and 0.95 confidence interval). Black lines indicate the periods of significant ( $p < 0.05$ ) linear trend.

productivity, as represented by  $\text{CHL}_{\text{tot}}$ . Starting in 2010, the PDO abruptly shifted from a cold to a warm phase, which in the northeastern Pacific resulted in enhanced stratification and a deepening of the upper mixed layer, thereby decreasing primary production, which we observed in our data set.

The effect of increasing PDO and decreasing NPGO on  $\text{CHL}$  in 2010–2015 was stronger than during a similar period around 1995, when the  $D_{\text{chl}}$  and nitracline deepened (cf. Figures 2d and 2f) but  $\text{CHL}_{\text{tot}}$  remained unchanged (Figure 2b). This may be linked to the increased range of PDO and NPGO fluctuations resulting from global warming (Sydeman et al., 2013). Other consequences of climate change in the study area may include the shoaling and strengthening of the California Undercurrent (Meinville & Johnson, 2013), a recent warm temperature anomaly in northeastern Pacific called “The Blob” (Bond et al., 2015; Di Lorenzo & Mantua, 2016), and extremely dry weather in California starting in 2011, with record drought in winter 2013/2014.

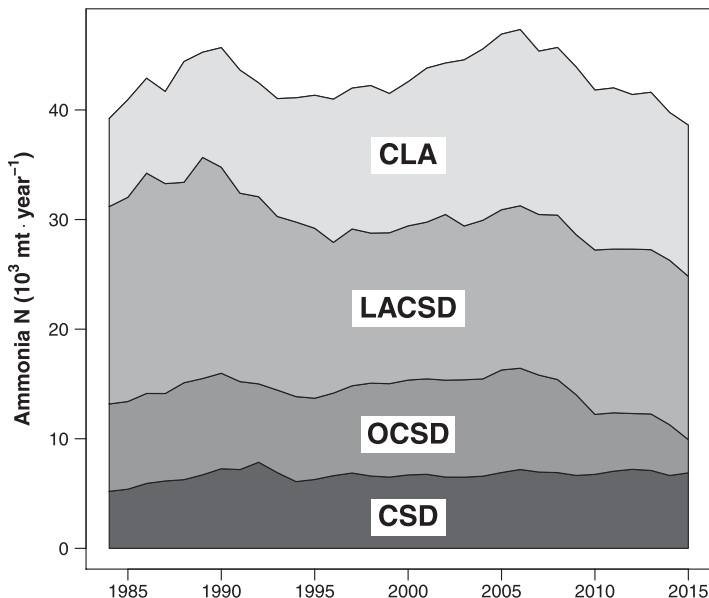


**Figure 9.** Stacked plot of ammonia nitrogen discharged from four major submerged POTW outfalls in southern California: City of Los Angeles (CLA), Sanitation Districts of Los Angeles County (LACSD), Orange County Sanitation District (OCSD), and City of San Diego (CSD).

The decrease of  $\text{CHL}_{\text{tot}}$  and deepening of  $D_{\text{chl}}$  during 2010–2015 was not observed in the northern coastal region of the SCB. Instead,  $\text{CHL}_{\text{tot}}$  in the northern region exhibited a weak, increasing trend over the entire time series between 1998 and 2005 (Figure 3b). The most likely reason for this pattern is that this region, more than other parts of the SCB, is affected by advection of waters upwelled off Point Conception (Bray et al., 1999; Hickey, 1993). The trends of  $\text{CHL}_{\text{tot}}$  in the upwelling zone likely differs from the central and southern parts of the SCB, which look more similar to the open ocean because the SCB is sheltered from northerly upwelling-generating winds by a coastal mountain range (Dorman & Winant, 1995). In contrast to the open ocean, the productivity of wind-generated coastal upwelling is expected to continue increasing (Bakun, 1990; Bakun et al., 2010; Di Lorenzo, 2015).

While this study demonstrates the critical role of North Pacific climatic cycles on the dynamics of phytoplankton biomass in the SCB, it does

not discount the local effect of anthropogenic nutrient inputs. Additionally, the recent decrease in CHL biomass in the central and southern SCB coincided in time with small but consistent decrease in the total volume of ammonia nitrogen discharged by the POTW outfalls (Figure 9). Also, the continuing growth of CHL<sub>tot</sub> in the northern SCB may be related to higher flux of ammonia nitrogen, compared to the central and southern coastal regions (Figure 9). Thus, while we see the same broad trends in the coastal shelf region as offshore, indicating a strong influence of Pacific Basin-scale drivers, the local, nearshore environment may still have an effect. Improved understanding about the magnitude of this effect needs further investigations including continued monitoring and numerical modeling.

### Acknowledgments

The authors wish to thank the field sampling personnel of the City of San Diego, Orange County Sanitation District, Sanitation Districts of Los Angeles County, City of Los Angeles, Southern California Coastal Water Research Project, and Aquatic Bioassay and Consulting Laboratories, without which this study would not have been possible. The data of water quality monitoring around POTW outfalls are available from SCCWRP website <http://hub.arcgis.com/datasets/scctrp::potw-wq-monitoring-ctd-data>. This work was supported by the Southern California Bight Regional Monitoring Program 2013 and a grant from the Sanitation Districts of Los Angeles County (grant JWSS-16-001).

### References

- Aksnes, D. L., & Ohman, M. D. (2009). Multi-decadal shoaling of the euphotic zone in the southern sector of the California Current System. *Limnology and Oceanography Methods*, 54(4), 1272–1281. <https://doi.org/10.4319/lom.2009.54.4.1272>
- Bakun, A. (1990). Global climate change and intensification of coastal ocean upwelling. *Science*, 247, 198–201. <https://doi.org/10.1126/science.247.4939.198>
- Bakun, A., Field, D. B., Redondo-Rodriguez, A., & Weeks, S. J. (2010). Greenhouse gas, upwelling-favorable winds, and the future of coastal ocean upwelling ecosystems. *Global Change Biology*, 16(4), 1213–1228. <https://doi.org/10.1111/j.1365-2486.2009.02094.x>
- Banse, K., & English, D. C. (1994). Seasonality of Coastal Zone Color Scanner phytoplankton pigment in the offshore oceans. *Journal of Geophysical Research*, 99(C4), 7323–7345. <https://doi.org/10.1029/93JC02155>
- Beckers, J.-M., & Rixen, M. (2003). EOF calculations and data filling from incomplete oceanographic datasets. *Journal of Atmospheric and Oceanic Technology*, 20(12), 1839–1856. [https://doi.org/10.1175/1520-0426\(2003\)020<1839:ECADFF>2.0.CO;2](https://doi.org/10.1175/1520-0426(2003)020<1839:ECADFF>2.0.CO;2)
- Behrenfeld, M. J., O'Malley, R. T., Siegel, D. A., McClain, C. R., Sarmiento, J. L., Feldman, G. C., ... Boss, E. S. (2006). Climate-driven trends in contemporary ocean productivity. *Nature*, 444(7120), 752–755. <https://doi.org/10.1038/nature05317>
- Bjorkstedt, E. P., Goericke, R., McClatchie, S., Weber, E., Watson, W., Lo, N., ... Abell, J. (2011). State of the California Current 2010–2011: Regionally variable responses to a strong (but fleeting?) La Niña. *California Cooperative Oceanic Fisheries Investigations Reports*, 52, 36–68.
- Bjorkstedt, E. P., Goericke, R., McClatchie, S., Weber, E., Watson, W., Lo, N., ... Abell, J. (2012). State of the California Current 2011–2012: Ecosystems respond to local forcing as La Niña Wavers and Wanes. *California Cooperative Oceanic Fisheries Investigations Reports*, 53, 41–76.
- Bograd, S. J., Buil, M. P., Di Lorenzo, E., Castro, C. G., Schroeder, I. D., Goericke, R., ... Whitney, F. A. (2015). Changes in source waters to the Southern California Bight. *Deep Sea Research Part II Topical Studies in Oceanography*, 112, 42–52. <https://doi.org/10.1016/j.dsrr.2014.04.009>
- Bond, N. A., Cronin, M. F., Freeland, H., & Mantua, N. J. (2015). Causes and impacts of the 2014 warm anomaly in the NE Pacific. *Geophysical Research Letters*, 42, 3414–3420. <https://doi.org/10.1002/2015GL063306>
- Booth, J. A. T., Woodson, C. B., Sutula, M. A., Micheli, F., Weisberg, S. B., Bograd, S. J., ... Crowder, L. B. (2014). Patterns and potential drivers of declining oxygen content along the southern California coast. *Limnology and Oceanography Methods*, 59(4), 1127–1138. <https://doi.org/10.4319/lo.2014.59.4.1127>
- Bray, N. A., Keyes, A., & Morawitz, W. M. L. (1999). The California Current system in the Southern California Bight and the Santa Barbara Channel. *Journal of Geophysical Research*, 104(C4), 7695–7714. <https://doi.org/10.1029/1998JC00038>
- Campbell, J. W. (1995). The lognormal-distribution as a model for biooptical variability in the sea. *Journal of Geophysical Research*, 100(C7), 13237–13254. <https://doi.org/10.1029/95JC00458>
- Carr, M. E., & Kearns, E. J. (2003). Production regimes in four Eastern Boundary Current systems. *Deep Sea Research Part II Topical Studies in Oceanography*, 50(22–26), 3199–3221. <https://doi.org/10.1016/j.dsrr.2003.07.015>
- Chao, Y., Ghil, M., & McWilliams, J. C. (2000). Pacific interdecadal variability in this century sea surface temperatures. *Geophysical Research Letters*, 27(15), 2261–2264. <https://doi.org/10.1029/1999GL011324>
- Cloern, J. E. (2001). Our evolving conceptual model of the coastal eutrophication problem. *Marine Ecology Progress Series*, 210, 223–253. <https://doi.org/10.3354/meps210223>
- Cullen, J. J. (2015). Subsurface chlorophyll maximum layers: Enduring enigma or mystery solved? *Annual Review of Marine Science*, 7, 207–239. <https://doi.org/10.1146/annurev-marine-010213-135111>
- Di Lorenzo, E. (2015). Climate science: The future of coastal ocean upwelling. *Nature*, 518(7539), 310–311. <https://doi.org/10.1038/518310a>
- Di Lorenzo, E., Combes, V., Keister, J. E., Strub, P. T., Thomas, A. C., Franks, P. J. S., ... Parada, C. (2013). Synthesis of Pacific Ocean climate and ecosystem dynamics. *Oceanography*, 26(4), 68–81. <https://doi.org/10.5670/oceanog.2013.76>
- Di Lorenzo, E., Fiechter, J., Schneider, N., Bracco, A., Miller, A. J., Franks, P. J. S., ... Hermann, A. J. (2009). Nutrient and salinity decadal variations in the central and eastern North Pacific. *Geophysical Research Letters*, 36, L14601. <https://doi.org/10.1029/2009GL038261>
- Di Lorenzo, E., & Mantua, N. J. (2016). Multi-year persistence of the 2014/15 North Pacific marine heatwave. *Nature Climate Change*, 6(11), 1042–1047. <https://doi.org/10.1038/nclimate3082>
- Di Lorenzo, E., Schneider, N., Cobb, K. M., Franks, P. J. S., Chhak, K., Miller, A. J., ... Riviere, P. (2008). North Pacific Gyre Oscillation links ocean climate and ecosystem change. *Geophysical Research Letters*, 35, L08607. <https://doi.org/10.1029/2007GL032838>
- Dorman, C. E. (1982). Winds between San Diego and San Clemente Island. *Journal of Geophysical Research*, 87(C12), 9636–9646. <https://doi.org/10.1029/JC087iC12p09636>
- Dorman, C. E., & Winant, C. D. (1995). Buoy observations of the atmosphere along the west coast of the United States. *Journal of Geophysical Research*, 100(C8), 16029–16044. <https://doi.org/10.1029/95JC00964>
- Dugdale, R. C. (1967). Nutrient limitation in the sea: Dynamics, identification, and significance. *Limnology and Oceanography*, 12(4), 685–695. <https://doi.org/10.4319/lo.1967.12.4.0685>
- Emery, W. J., & Thomson, R. E. (2014). *Data analysis methods in physical oceanography*. Amsterdam, The Netherlands: Elsevier Science.
- Flament, P. (2002). A state variable for characterizing water masses and their diffusive stability: Spiciness. *Progress in Oceanography*, 54(1–4), 493–501. [https://doi.org/10.1016/S0079-6611\(02\)00065-4](https://doi.org/10.1016/S0079-6611(02)00065-4)
- Freeland, H., Denman, K., Wong, C. S., Whitney, F., & Jacques, R. (1997). Evidence of change in the winter mixed layer in the Northeast Pacific Ocean. *Deep Sea Research Part I Oceanographic Research Papers*, 44(12), 2117–2129. [https://doi.org/10.1016/S0967-0637\(97\)00083-6](https://doi.org/10.1016/S0967-0637(97)00083-6)

- Hastie, T., & Tibshirani, R. (1986). Generalized additive models. *Statistical Science*, 1(3), 297–310. <https://doi.org/10.1214/ss/1177013604>
- Hayward, T. L., Baumgartner, T. R., Checkley, D. M., Durazo, R., Gaxiola-Castro, G., Hyrenbach, K. D., ... Tegner, M. J. (1999). The state of the California Current in 1998–1999: Transition to cool-water conditions. *California Cooperative Oceanic Fisheries Investigations Reports*, 40, 29–62.
- Hickey, B. M. (1979). The California Current system: Hypotheses and facts. *Progress in Oceanography*, 8, 191–279. [https://doi.org/10.1016/0079-6611\(79\)90002-8](https://doi.org/10.1016/0079-6611(79)90002-8)
- Hickey, B. M. (1992). Circulation over the Santa Monica-San Pedro basin and shelf. *Progress in Oceanography*, 30, 37–115. [https://doi.org/10.1016/0079-6611\(92\)90009-O](https://doi.org/10.1016/0079-6611(92)90009-O)
- Hickey, B. M. (1993). Physical oceanography. In M. D. Dailey, D. J. Reish, & J. W. Anderson (Eds.), *Ecology of the Southern California Bight* (pp. 19–70). Berkeley, CA: University of California Press.
- Howard, M. D. A., Sutula, M., Caron, D. A., Chao, Y., Farrara, J. D., Frenzel, H., ... Sengupta, A. (2014). Anthropogenic nutrient sources rival natural sources on small scales in the coastal waters of the Southern California Bight. *Limnology and Oceanography Methods*, 59(1), 285–297. <https://doi.org/10.4319/lom.2014.59.1.0285>
- Kahru, M., Kudela, R. M., Manzano-Sarabia, M., & Mitchell, B. G. (2012). Trends in the surface chlorophyll of the California Current: Merging data from multiple ocean color satellites. *Deep Sea Research Part II: Topical Studies in Oceanography*, 77–80, 89–98. <https://doi.org/10.1016/j.dsrr.2012.04.007>
- Kelley, D., & Richards, C. (2017). oce: Analysis of Oceanographic Data. R package version 0.9–21. Retrieved from <https://CRAN.R-project.org/package=oce>
- Kilduff, D. P., Di Lorenzo, E., Botsford, L. W., & Teo, S. L. H. (2015). Changing central Pacific El Niños reduce stability of North American salmon survival rates. *Proceedings of the National Academy of Sciences of the United States of America*, 112(35), 10962–10966. <https://doi.org/10.1073/pnas.1503190112>
- Kim, H.-J., & Miller, A. J. (2007). Did the thermocline deepen in the California Current after the 1976/77 climate regime shift? *Journal of Physical Oceanography*, 37(6), 1733–1739. <https://doi.org/10.1175/JPO3058.1>
- Koch, S. E., desJardins, M., & Kocin, P. J. (1983). An interactive Barnes objective map analysis scheme for use with satellite and conventional data. *Journal of Climatology and Applied Meteorology*, 22(9), 1487–1503. [https://doi.org/10.1175/1520-0450\(1983\)022<1487:AIBOMA>2.0.CO;2](https://doi.org/10.1175/1520-0450(1983)022<1487:AIBOMA>2.0.CO;2)
- Leinweber, A., & Gruber, N. (2013). Variability and trends of ocean acidification in the Southern California Current System: A time series from Santa Monica Bay. *Journal of Geophysical Research: Oceans*, 118, 3622–3633. <https://doi.org/10.1002/jgrc.20259>
- Longhurst, A. R. (1995). Seasonal cycles of pelagic production and consumption. *Progress in Oceanography*, 36(2), 77–167. [https://doi.org/10.1016/0079-6611\(95\)00015-1](https://doi.org/10.1016/0079-6611(95)00015-1)
- Lynn, R. J., & Simpson, J. J. (1987). The California Current System: The seasonal variability of its physical characteristics. *Journal of Geophysical Research*, 92(C12), 12947–12966. <https://doi.org/10.1029/JC092iC12p12947>
- Lyon, G. S., Petschauer, D., & Stein, E. D. (2006). *Effluent discharges to the Southern California Bight from large municipal wastewater treatment facilities in 2003 and 2004*. Westminster, CA. Retrieved from [ftp://ftp.sccwrp.org/pub/download/DOCUMENTS/AnnualReports/2005\\_06AnnualReport/AR0506\\_001-16.pdf](ftp://ftp.sccwrp.org/pub/download/DOCUMENTS/AnnualReports/2005_06AnnualReport/AR0506_001-16.pdf)
- Lyon, G. S., & Stein, E. D. (2008). *Effluent discharges to the Southern California Bight from small municipal wastewater treatment facilities in 2005*. Costa Mesa, CA. Retrieved from [ftp://ftp.sccwrp.org/pub/download/DOCUMENTS/AnnualReports/2008AnnualReport/AR08\\_001\\_014.pdf](ftp://ftp.sccwrp.org/pub/download/DOCUMENTS/AnnualReports/2008AnnualReport/AR08_001_014.pdf)
- Mantua, N. J., Hare, S. R., Zhang, Y., Wallace, J. M., & Francis, R. C. (1997). A Pacific Interdecadal Climate Oscillation with impacts on salmon production. *Bulletin of the American Meteorological Society*, 78(6), 1069–1079. [https://doi.org/10.1175/1520-0477\(1997\)078<1069:APICOW>2.0.CO;2](https://doi.org/10.1175/1520-0477(1997)078<1069:APICOW>2.0.CO;2)
- McClatchie, S., Goericke, R., Leising, A., Auth, T. D., Bjorkstedt, E., Robertson, R. R., ... Jahncke, J. (2016). State of the California Current 2015–16: Comparisons with the 1997–98 El Niño. *California Cooperative Oceanic Fisheries Investigations Reports*, 57.
- Meinvielle, M., & Johnson, G. C. (2013). Decadal water-property trends in the California Undercurrent, with implications for ocean acidification. *Journal of Geophysical Research: Oceans*, 118, 6687–6703. <https://doi.org/10.1002/2013JC009299>
- Messie, M., & Chavez, F. P. (2015). Seasonal regulation of primary production in eastern boundary upwelling systems. *Progress in Oceanography*, 134, 1–18. <https://doi.org/10.1016/j.pocean.2014.10.011>
- Miller, A. J., & Schneider, N. (2000). Interdecadal climate regime dynamics in the North Pacific Ocean: Theories, observations and ecosystem impacts. *Progress in Oceanography*, 47(2–4), 355–379. [https://doi.org/10.1016/S0079-6611\(00\)00044-6](https://doi.org/10.1016/S0079-6611(00)00044-6)
- Newman, M., Alexander, M. A., Ault, T. R., Cobb, K. M., Deser, C., Di Lorenzo, E., ... Smith, C. A. (2016). The Pacific Decadal Oscillation, revisited. *Journal of Climate*, 29(12), 4399–4427. <https://doi.org/10.1175/JCLI-D-15-0508.1>
- Nezlin, N. P., Sutula, M. A., Stumpf, R. P., & Sengupta, A. (2012). Phytoplankton blooms detected by SeaWiFS along the central and southern California coast. *Journal of Geophysical Research*, 117, C07004. <https://doi.org/10.1029/2011JC00773>
- Papadakis, J. E. (1981). *Determination of the wind mixed layer by an extension of Newton's method*. Sidney, BC. Retrieved from <http://www.dfo-mpo.gc.ca/Library/58484.pdf>
- Parsons, T. R., Maita, Y., & Lalli, C. M. (1984). *A manual of chemical and biological methods for seawater analysis* (1st ed.). Oxford, UK: Pergamon Press.
- Patti, B., Guisande, C., Vergara, A. R., Riveiro, I., Maneiro, I., Barreiro, A., ... Mazzola, S. (2008). Factors responsible for the differences in satellite-based chlorophyll a concentration between the major global upwelling areas. *Estuarine Coastal and Shelf Science*, 76(4), 775–786. <https://doi.org/10.1016/j.ecss.2007.08.005>
- Pebesma, E. J. (2004). Multivariable geostatistics in S: The gstat package. *Computers & Geosciences*, 30(7), 683–691. <https://doi.org/10.1016/j.cageo.2004.03.012>
- Pebesma, E. J. (2012). Spacetime: Spatio-temporal data in R. *Journal of Statistical Software*, 51(7). <https://doi.org/10.18637/jss.v051.i07>
- Peterson, W. T., & Schwing, F. B. (2003). A new climate regime in Northeast Pacific ecosystem. *Geophysical Research Letters*, 30(17), 1896. <https://doi.org/10.1029/2003GL017528>
- Philander, G. (1990). *El Niño, La Niña and the southern oscillation*. San Diego, CA: Academic Press.
- Polovina, J. J., Dunne, J. P., Woodworth, P. A., & Howell, E. A. (2011). Projected expansion of the subtropical biome and contraction of the temperate and equatorial upwelling biomes in the North Pacific under global warming. *ICES Journal of Marine Science*, 68(6), 986–995. <https://doi.org/10.1093/icesjms/fsq198>
- Polovina, J. J., Howell, E. A., & Abecassis, M. (2008). Ocean's least productive waters are expanding. *Geophysical Research Letters*, 35, L03618. <https://doi.org/10.1029/2007GL031745>
- Preisendorfer, R. W. (1988). *Principal component analysis in meteorology and oceanography*. New York, NY: Elsevier Science.

- Riley, G. A. (1946). Factors controlling phytoplankton population on Georges Bank. *Journal of Marine Research*, 6(1), 54–73.
- Roemmich, D., & McGowan, J. A. (1995). Climatic warming and the decline of zooplankton in the California Current. *Science*, 267(5202), 1324–1326. <https://doi.org/10.1126/science.267.5202.1324>
- Rykaczewski, R. R., & Dunne, J. P. (2010). Enhanced nutrient supply to the California Current ecosystem with global warming and increased stratification in an earth system model. *Geophysical Research Letters*, 37, L21606. <https://doi.org/10.1029/2010GL045019>
- Sarmiento, J. L., Slater, R., Barber, R., Bopp, L., Doney, S. C., Hirst, A. C., ... Stouffer, R. (2004). Response of ocean ecosystems to climate warming. *Global Biogeochemical Cycles*, 18, GB3003. <https://doi.org/10.1029/2003GB002134>
- Simpson, G. (2014). Identifying periods of change in time series with GAMs. Retrieved from <http://www.fromthebottomoftheheap.net/2014/05/15/identifying-periods-of-change-with-gams/>
- Simpson, G. (2017). tsgam: Utilities for Working with GAMs Fitted to Time Series. R package version 0.0–2. Retrieved from <https://github.com/gavin Simpson/tsgam>
- Stein, E. D., & Cadien, D. B. (2009). Ecosystem response to regulatory and management actions: The southern California experience in long-term monitoring. *Marine Pollution Bulletin*, 59(4–7), 91–100. <https://doi.org/10.1016/j.marpolbul.2009.02.025>
- Steinacher, M., Joos, F., Frolicher, T. L., Bopp, L., Cadule, P., Cocco, V., ... Segschneider, J. (2010). Projected 21st century decrease in marine productivity: A multi-model analysis. *Biogeosciences*, 7(3), 979–1005. <https://doi.org/10.5194/bg-7-979-2010>
- Sverdrup, H. U., & Fleming, R. H. (1941). The waters off the coast of southern California, March to July 1937. *Bulletin of the Scripps Institution of Oceanography Technical Series*, 4, 261–378.
- Syde man, W. J., Santora, J. A., Thompson, S. A., Marinovic, B., & Di Lorenzo, E. (2013). Increasing variance in North Pacific climate relates to unprecedented ecosystem variability off California. *Global Change Biology*, 19(6), 1662–1675. <https://doi.org/10.1111/gcb.12165>
- Thomson, R. E., & Fine, I. V. (2003). Estimating mixed layer depth from oceanic profile data. *Journal of Atmospheric and Oceanic Technology*, 20(2), 319–329. [https://doi.org/10.1175/1520-0426\(2003\)020<0319:EMLDFO>2.0.CO;2](https://doi.org/10.1175/1520-0426(2003)020<0319:EMLDFO>2.0.CO;2)
- Trenberth, K. E. (1997). The definition of El Niño. *Bulletin of the American Meteorological Society*, 78(12), 2771–2777. [https://doi.org/10.1175/1520-0477\(1997\)078<2771:TDOENO>2.0.CO;2](https://doi.org/10.1175/1520-0477(1997)078<2771:TDOENO>2.0.CO;2)
- Wang, S., Huang, J., He, Y., & Guan, Y. (2014). Combined effects of the Pacific Decadal Oscillation and El Niño-Southern Oscillation on global land dry-wet changes. *Scientific Reports*, 4, 6651. <https://doi.org/10.1038/srep06651>
- Wood, S. N. (2016). Just another Gibbs additive modeler: Interfacing JAGS and MGCV. *Journal of Statistical Software*, 75(7), 1–15. <https://doi.org/10.18637/jss.v075.i07>
- Zhang, Y., Wallace, J. M., & Battisti, D. S. (1997). ENSO-like interdecadal variability: 1900–93. *Journal of Climate*, 10(5), 1004–1020. [https://doi.org/10.1175/1520-0442\(1997\)010<1004:ELIV>2.0.CO;2](https://doi.org/10.1175/1520-0442(1997)010<1004:ELIV>2.0.CO;2)